Carbohydrate Polymers 119 (2015) 202–209

Contents lists available at ScienceDirect

Carbohydrate Polymers

journal homepage: www.elsevier.com/locate/carbpol

Fabrication and characterization of nanofibrillated cellulose and its aerogels from natural pine needles

Shaoliang Xiao[a], Runan Gao[a], Yun Lu[b,*], Jian Li[a,*], Qingfeng Sun[a,*]

[a] Material Science and Engineering College, Northeast Forestry University, Harbin 150040, China
[b] Research Institute of Wood Industry, Chinese Academy of Forestry, Beijing 100091, China

ARTICLE INFO

Article history:
Received 23 August 2014
Received in revised form
11 November 2014
Accepted 19 November 2014
Available online 27 November 2014

Keywords:
Aerogels
Nanofibrillated cellulose
Pine needles
Ultrasonic
Hydrophobic

ABSTRACT

To obtain the nanofibriled cellulose from natural pine needles, a combination of chemical pretreatments and subsequently ultrasonic treatments was employed for removing the hemicelluloses and lignins and splitting the bundled cellulose into pine needle nanofibers. Using SEM and diameter distribution method, it was confirmed that the obtained pine needle nanofibers had a narrow diameter from 30 to 70 nm. The crystalline type of the pine needle nanofibers was the cellulose I type. The crystallinity reached 66.19%, which was increased by 7.61% as compared with the raw material pine needles. The TGA and DTG results showed that the degradation temperature of the nanofibers was increased to approximately 267 and 352 °C compared with 221 and 343 °C of the raw material fibers, respectively. Furthermore, the highly flexible and ultralight pine needle nanofibers aerogels were prepared from the aqueous pine needle nanofibers solution using the freezing-drying technique. Aerogels were studied by SEM observation and nitrogen gas adsorption. The mechanical properties were measured in compression for aerogels. This study provides a new opportunity to fabricate novel nanomaterials from waste biomass materials, which is crucial for the fully utilizing of abundant biomass resources.

1. Introduction

It is well-known that cellulose, which accounts for approximately 40% of plant biomass, is the most abundant biopolymer in the world. Interest has recently arisen in the utilization of cellulose due to its unique characteristics, such as biodegradability, biocompatibility, renewability, and sustainability (Ifuku & Saimoto, 2012). Especially an increasing attention is being devoted to the nanometer-sized single cellulose fibers, generally defined as fibers with a diameter below 100 nm (Li & Xia, 2004; Sun, Mayers, Herricks, & Xia, 2003), because of their intrinsic properties, such as the nanoscale dimensions, high surface area, unique morphology, low density and high mechanical strength (Habibi, Lucia, & Rojas, 2010). A great number of applications of nanometer-sized single cellulose fibers, such as the controlled drug release formulations (Valo et al., 2013), food presentation (Klemm et al., 2011), tissue engineering (Bodin et al., 2007), cosmetics (Klemm et al., 2006), biodegradable packaging materials (Khan et al., 2010), reinforcement components in flexible display panels and oxygen-barrier layers (Shinoda, Saito, Okita, & Isogai, 2012), were undertaken. Therefore, the development of effective methods for extracting nanofibers from biomass has received an arising interest. The existing approaches include mechanical, chemical and biological treatments (Chen, Liu, Chang, Cao, & Anderson, 2009), TEMPO-mediated oxidation on the surface of microfibrils and a subsequent mild mechanical treatment, electrospinning methods (Zhang & Yu, 2014), and ultrasound treatment (Huang, Zhang, Kotaki, & Ramakrishna, 2003; Kim, Kim, Kang, Marquez, & Joo, 2006). Among these methods, ultrasound for materials synthesis has been sufficiently investigated and is considered as one of the most powerful tools in nanostructured materials synthesis (Bang & Suslick, 2010; Zeiger & Suslick, 2011). The chemical effect of ultrasonication is caused by acoustic cavitation, which generates localized hot spots with very high temperatures (>5000 K), pressures (>20 MPa), and heating/cooling rates (>1010 K/s) (Suslick, 1998). Such extreme environments provide a unique platform to break the strong cellulose interfibrillar hydrogen bonding, allowing nanofibers to be gradually disintegrated (Cheng, Wang, & Han, 2010; Tischer, Sierakowski, Westfahl, & Tischer, 2010; Zhao, Feng, & Gao, 2007). Furthermore, this isolation technology may be universally applicable to all the biomass resources consisting of nanofibers and

* Corresponding author at: Northeast Forestry University, No. 26 Hexing Road, Xiangfang District, Harbin 150040, China. Tel.: +86 451 82192399; fax: +86 451 82192399.
E-mail addresses: luyun@criwi.org.cn (Y. Lu), jianli@nefu.edu.cn (J. Li), qfsun@nefu.edu.cn (Q. Sun).

http://dx.doi.org/10.1016/j.carbpol.2014.11.041
0144-8617/

other embedding matrixes (Lu et al., 2013). Accordingly, this study investigates the extraction of natural pine needle nanofibers from natural pine needles under pulsed ultrasonication.

Pine needles are a renewable natural bioresource and abundant across all China. With several advantages including rapid growth, renewability, relatively high strength, and good flexibility, pine needles can be harvested all the year round and one ton needles can be collected in two acres of pine generally (Thakur & Singha, 2011). Pine needle is composed of approximately 30% cellulose, 23% lignin and others substrates. The previous studies on cellulose nanofibers that were extracted from the pine needles by a chemical–mechanical technique were reported to examine their potential applications.

Plant cell walls usually consist of rigid cellulosic microfibrils embedded in the soft hemicelluloses and lignin matrix. Cellulose is the fibrillar component of plant cells, which are, however, tightly hooked to one another by multiple hydrogen bonds. Moreover, cellulose nanofibers are embedded in matrix substances such as hemicellulose and lignin in cell walls. Thus it is difficult to split cellulose fibrils only by mechanical treatments (Saito, Kimura, Nishiyama, & Isogai, 2007). Many researchers reported that the matrix substances were removed using chemical methods before the fibrillation process and kept the material in the water-swollen state. As a result, the narrow cellulose nanofibers can be obtained. Herein, a successful process of cellulose fiber nano-fibrillation from pine needles using the facile pulsed ultrasonication combined with chemical pretreatments was reported. The process could yield high-crystallinity and high-quantity pine needle nanofibers with a narrow width ranging from 30 to 70 nm (Abe, Iwamoto, & Yano, 2007; Alemdar & Sain, 2008b; Lu et al., 2013). This high-intensity ultrasonication treatment can separate nanofibers from natural nanofiber-embedding matrixes after the removal of the matrix substances. More interestingly, ultralight and highly flexible cellulose nanoporous aerogels were also prepared from narrow diameter distribution nanofibers using vacuum freezing-drying technique. Additionally, Cervin et al. reported a type of hydrophobic and oleophilic NFC aerogels for oil/water separation via a vapor phase deposition method, which is considerably simple, feasible and facile (Cervin, Aulin, Larsson, & Wågberg, 2012). In the present work, the hydrophilic and the hydrophobic NFC aerogels from natural pine needles were both fabricated and their own features were also characterized. The hydrophobic NFC aerogel from natural pine needles showed superior oil/water separation.

2. Materials and methods

2.1. Raw materials

The pine needle powder with a 60 mesh was used for the analysis of cellulose nanofibers. 2 g dried powder was extracted with benzene/ethanol (2:1,v:v) in soxhlet 90 °C for 6 h. The dewaxed samples were dried in an oven for 24 h at 50 °C before use. Potassium hydroxide (KOH), hydrochloric acid (HCl), ethanol, benzene, acetic acid, sodium chlorite, trimethylchlorosilane and other chemicals used were of the analytical or reagent grade.

2.2. Preparation of pine needle nanofibers

The isolation process consist of a series of chemical treatments in Fig. 1. and high-intensity ultrasonication according to the flowchart shown in Fig. 2. First, acidified sodium chlorite treatment was carried out at 75 °C for 1 h, which was repeated five times until the product became white. Following the method of Abe and Yano (2009), the major lignin was removed. Next, an alkaline treatment with potassium hydroxide (KOH) was conducted for removing the

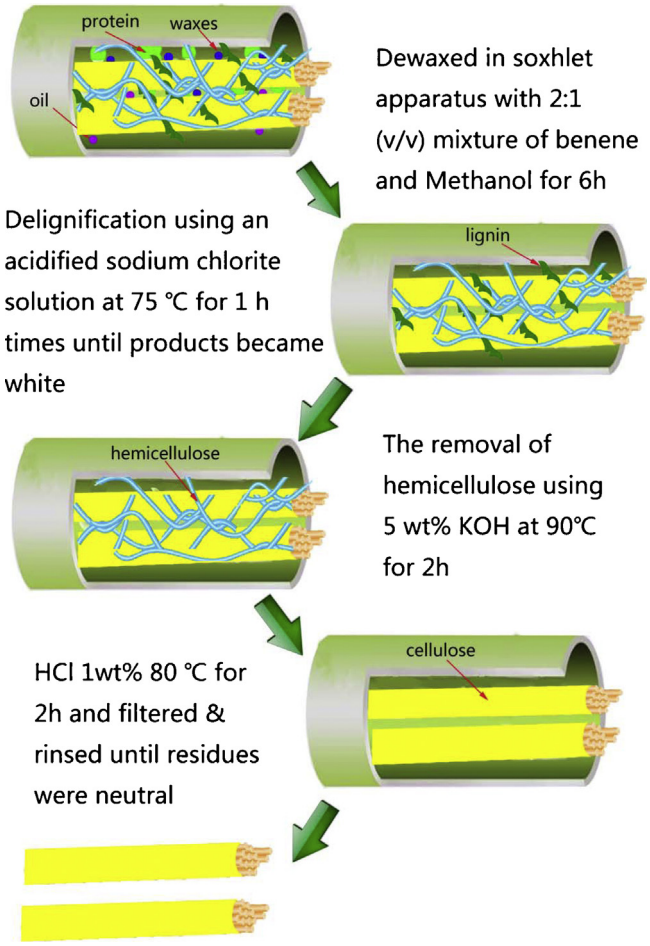

Fig. 1. The isolation process of a series of chemical treatment.

hemicelluloses, residual starch and pectin. Then the samples were treated using the hydrochloric acid (HCl) at 80 °C for 2 h. After the series of chemical treatments, the samples were filtered and rinsed with distilled water until the residues were neutralized. The samples were kept in a water-swollen state during the whole chemical process to avoid generating strong hydrogen bonding among nanofibers after the matrix was removed.

The purified pine needle microfibrils with a diameter ranging from 6 to 18 μm were split to thinner pine needle fibrils after 30 min ultrasonic treatment along the axes of the fibers. All these pine needle fibrils are further separated to 30–70 nm width nanofibers.

After the chemical pretreatment, to facilitate nanofibrillation, the purified cellulose fibers were dispersed in distilled water such that approximately 450 mL of the water slurry contained 0.5 wt% samples. Sonication was performed at 60 kHz with a Sonifiers® Cell Disruptor/Homogenizer (JY99-IID, Scientz Technology, China) with a 1-cm^2-diameter titanium horn under a 50% duty cycle (i.e., a repeating cycle of 0.5-s ultrasonic treatment and 0.5-s shutdown) to

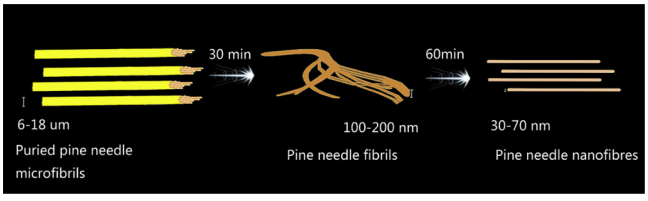

Fig. 2. The individualization of pine needle nanofibers from pine needle powers with a typical laboratory-scale ultrasonication apparatus under neutral condition.

reduce temperature variation. The sonication then was conducted for 1 h with an output power of 1500 W to isolate the fibers. The ultrasonic treatment was carried out in an ice/water bath, and the ice was maintained throughout the entire ultrasonication time.

2.3. Preparation of pine needle nanofibers aerogels

The pine needle nanofibers suspensions were poured into molds and then placed in a refrigerator. Next, the frozen samples were freeze-dried using a Scientz-10 N freeze-dryer (BT6K-ES, Virtis) to sublime the materials directly from the solid phase to the gas phase. The cold trap temperature was below −55 °C and the vacuum pressure was below 25 μPa during the freeze-drying process. The freeze-dried pine needle nanofiber aerogels were used for the characterization.

2.4. Hydrophobic coating of pine needle nanofibers aerogels

The hydrophilic pine needle nanofibers aerogels were obtained by the treatment of trimethylchlorosilane through the vapor phase deposition. The aerogels were placed in big glass bottle. A small glass vial containing trimethylchlorosilane was added into the glass bottle. Within the desiccator, the sample and trimethylchlorosilane allowed to react for 48 h at ambient temperature. This process successfully fabricated hydrophobic aerogels.

2.5. Characterization

Surface morphology of specimens was characterized by the field emission scanning electron microscopy (SEM, FEI, Sirion 200) operating at 20.0 kV. The chemical analysis was accomplished using the energy dispersive X-ray spectroscopy (EDXA) in connection with SEM and by FTIR spectroscopy (MagnaIR 560, Nicolet, KBr method). X-ray diffraction (XRD: Bruker D8 Advance, Germany) operating with Cu-K αradiation (λ = 1.5418 Å) at a scan rate of 4°/min, 40 kV, 40 mA ranging from 5° to 60°. The thermal stability was characterized by TG analyzer (TA, Q600) from 25 to 800 °C with a heating rate of 10 °C min^{-1} under nitrogen atmosphere. Water contact angle (WCA) was measured on an OCA40 contact angle system (Dataphysics, Germany) at room temperature. The final value of the CA was obtained as an average of five measurements. The specific surface area using Brunauer–Emmett–Teller (BET) analysis and nitrogen adsorption/desorption isotherms of the aerogels were determined by Brunauer–Emmett–Teller (BET) analysis via an accelerated surface area and porosimetry system (3H-2000PS2 unit, Beishide Instrument S & T Co., Ltd.). Approximately 0.1 g of aerogel sample was first degassed in instrument at 105 °C for 4 h prior to the analysis followed by N_2 adsorption at −196 °C. The BET surface area and the BJH pore size distribution were calculated. The compressive strength of the aerogel samples with a cylindrical shape was evaluated by an electronic universal mechanical testing machine (RGT-20A, Qingdao, China), which is equipped with a load cell of 500 N load cell at a strain rate of 10% min^{-1} in a conditioned room at 24 °C and 64% relative humidity.

3. Results and discussion

3.1. Examination of pine needle nanofibers

Fig. 3a shows the microstructure of the cross-section of the original materials. The microstructure of the pine needle was of an outer epidermis and the cellular structure. The epidermis was rich in cellulose (Hornsby, Hinrichsen, & Tarverdi, 1997). Intercellular material consisted of lignin, hemicelluloses and extractives (waxes, oil, pectin, etc.), which were the cementing materials around the fiber-bundles. Fig. 3b shows the structure of the pine needle fibers after the chemical treatment. The chemical-purified cellulose with cleaner surface suggested that the hemicelluloses, lignin and extractives were partially removed after a series of chemical pretreatments in Fig. 1. The pine needle fibers were separated into individual micro-sized fibers with the mean diameter of 12.43 μm (Fig. 2e). In fact, these microsized fibers were reportedly composed of strong hydrogen bonding nanofibers, and individualized nanofiber bundles with a width of 30–70 nm can be seen in Fig. 3f. Fig. 3c shows SEM images of the sample after ultrasonic treatment, yielding plentiful slender fibrils. It is clear that from the image the average diameter of the fibers is about 50.91 nm (Fig. 3f). The insert graph of Fig. 3a shows the nanofibers without any chemical treatment which was directly by treated by the ultrasonication. Furthermore, the morphology structure of aerogels before and after vapor phase deposition are shown in Fig. S1. The NFCs apparently were interconnected with each other and formed a typical porous three dimensional network (3D) structure, which suggested the NFC aerogel would be a potential substrate for 3D functional materials (Cervin et al., 2013; Zhang, Sèbe, Rentsch, Zimmermann, & Tingaut, 2014). The elemental compositions in the samples were detected by an energy dispersive X-ray spectroscopy (EDXA). The EDXA spectra (as shown in Fig. 2d, insets in Fig. 3e and f) show the peaks for C, N, O, K, Ca, Mg, and P according to their binding energies, respectively. The main components contain C (48.77 wt%), O (26.87 wt%) and N (18.54 wt%) in the raw material. The inorganic elements in the raw material contain K (1.13 wt%), Ca (1.44 wt%), Mg (0.31 wt%), and P (2.95 wt%). Additionally, the peaks of N, K, Ca, Mg and P disappeared in the EDXA spectra of the samples (insets in Fig. 3e and f), indicating that these substances had been completely removed during the chemical pretreatment process.

Their compact agglomeration of pine needle nanofibers showed that cellulose chains had an intermolecular hydrogen bonding and a strong hydrophilic interaction in between the cellulosic chains. It may be explained by the effect of acoustic cavitation of high frequency (20–25 kHz) ultrasound in the formation, expansion, and implosion of microbubbles in aqueous solution. This violent collapse caused direct particle-shock wave interactions and was the primary pathway to split pine needle cellulose fibers along the axial direction. Thus, the sonification impact broke the relatively weak pine needle interfibrillar hydrogen bonding and the Van der Waals force, gradually disintegrating the micro-scale pine needle fibers into nanofibers. (Lu et al., 2013; Zeiger & Suslick, 2011; Zhao et al., 2007) The ultrasonic treatment method was an efficient pathway to prepare ultrafine nanofibrils from pine needle microfibres.

3.2. Characterizations of the samples

Cellulose crystallinity in the samples played a key role in the determination of the mechanical and thermal properties. To obtain the crystallinity of the samples and analyze the effect of chemical pretreatment and ultrasonic treatment on the reorganization of pine needle nanofibers, the XRD examination was carried out. Fig. 4 shows the diffractograms of (a) the raw materials, (b) chemical-purified cellulose fibers, and (c) nanofibers. All samples exhibited sharp diffraction peaks around $2\theta = 14.8°$ (1 0 1), 16.5° (1 0 *i*) and 22.5° (0 0 2) (Kim et al., 2006), which are supposed to represent the typical cellulose-I structure (Nishiyama, Sugiyama, Chanzy, & Langan, 2003). This suggested that the crystal structure of cellulose was not changed during the preparation. Moreover, Fig. 4a shows the XRD pattern of the raw materials. The diffraction peaks at $2\theta = 14.75$ (2 0 0), 24.37 (0 0 4), 29.86 (2 1 4), 31.14 (1 2 4), 35.45 (0 4 0), and 38.10 (3 0 5) can be assigned to the phase of $Mg(NH_4)_2H_2(PO_4)_2{\cdot}4H_2O$ (JCPDF 16-0353), $C_2CaO_4{\cdot}H_2O$ (JCPDF 20-0231) and $K_2CaP_4O_{12}$ (JCPDF 29-0992). These mineral crystals were all removed from the raw materials by the potassium hydroxide (KOH) and the hydrochloric acid (HCl) treatment. The

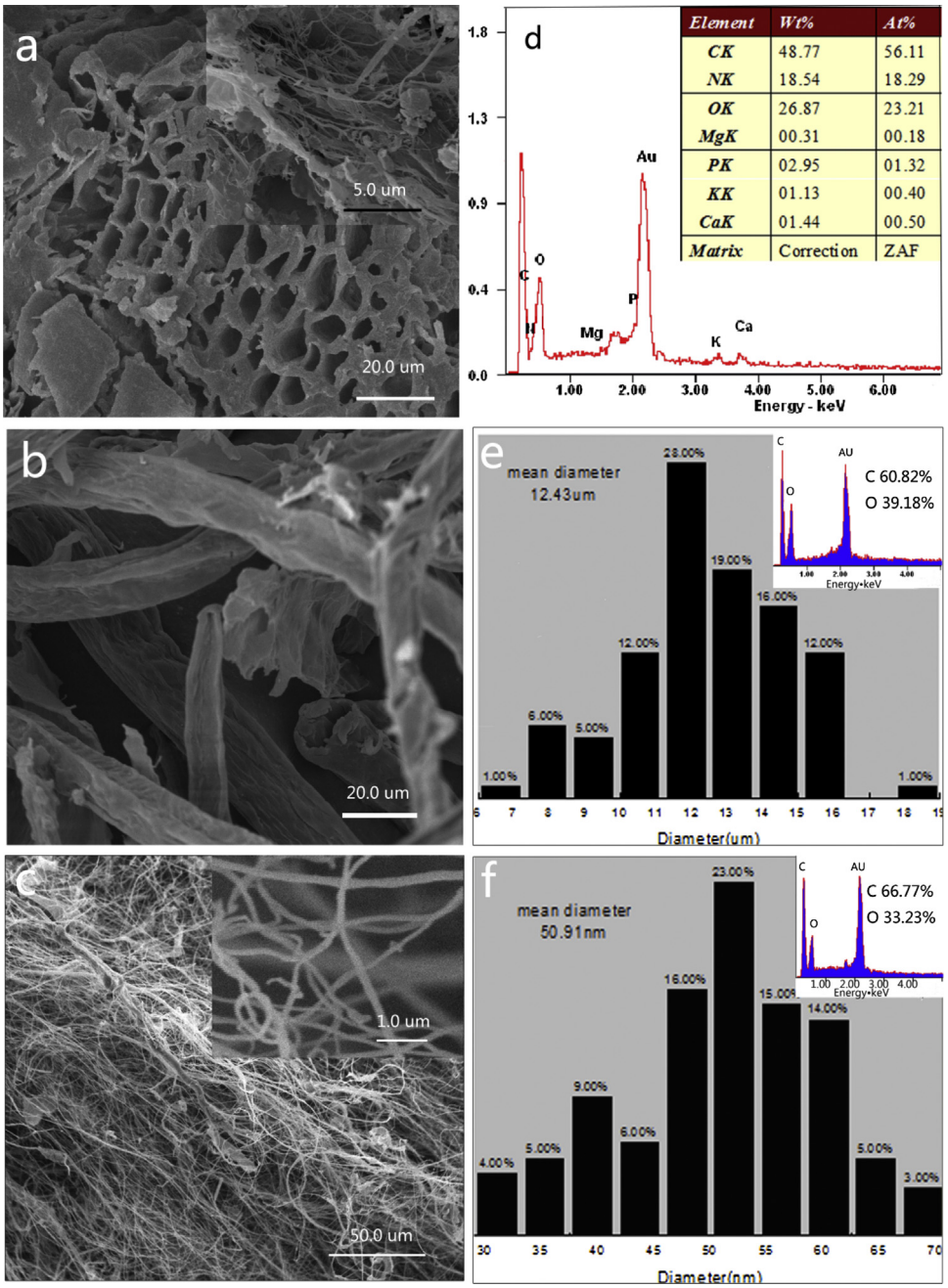

Fig. 3. SEM micrographs of (a) the raw materials, the insets of SEM graphs are the raw materials nanofibers using directly ultrasonic treatment without any chemical pretreatment. (b) The chemical-purified cellulose. (d) The energy dispersive X-ray spectroscopy (EDXA) of the raw materials, (e), and (f) are the corresponding diameter distributions of the fibers of (b), (c), and insets are corresponding the EDS spectra, respectively.

crystallinity of each sample was also calculated according the Segal method and is listed in Table 1. The crystallinity values were estimated as 58.58, 71.14 and 66.19% for (a) the raw materials, (b) chemical-purified cellulose fibers, and (c) nanofibers, respectively.

Table 1
The crystallinity of the pine needle cellulose sample.

Sample	I_{002}	I_{am}	Relative crystallinity (%)
The raw materials	458	324	58.58
Chemical-purified cellulose	742	301	71.14
Pine needle nanofibers	276	141	66.19

The increase in crystallinity after chemical pretreatment was due to the removal of the most hemicelluloses which exist in the amorphous regions and was reported by several authors (Alemdar & Sain, 2008b; Li et al., 2009). This leaded to the realignment of cellulose molecules. However, after ultrasonic treatment, the crystallinity of nanofibers was lower than that of the chemical-purified cellulose fibers, which implied that the ultrasonic treatment had an effect on the destruction of the crystal regions in the cellulose nanofibers. It was probably explained that the energy release during the cavitation processes made the aligned microfibril unparallel and transferred to the hydrogen junction zones along the microfibril direction (Chen et al., 2013). The increase in the number of crystallinity regions increased the rigidity of cellulose, leading higher tensile strength of the fibers. Therefore it was more effective

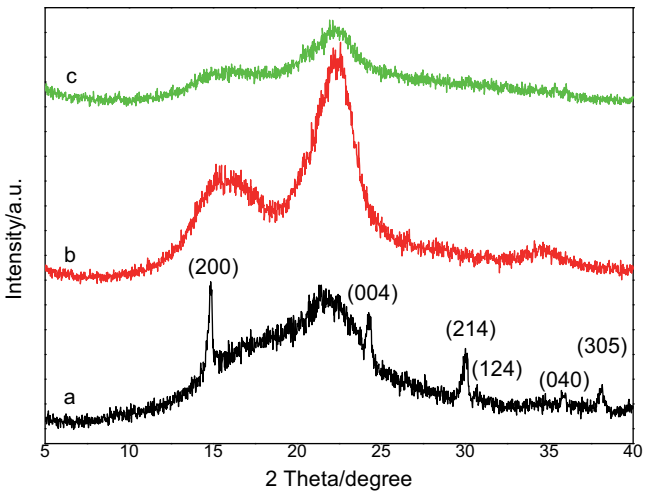

Fig. 4. X-ray diffraction patterns of (a) the raw materials, (b) chemical-purified cellulose fibers, and (c) pine needle nanofibers.

Table 2
Frequencies (cm^{-1}) of the main signals of (a) the raw materials, (b) purified pine needle fibers, (c) pine needle nanofibers and the assignments.

Absorption band (cm^{-1})	Assignment
3325–3340 (m)	O—H stretch (hydrogen-bonded)
2889–2915 (m)	C—H stretching
1727 (m)	Alkyl esther from cell wall hemicellulose C=O; strong carbonyl groups in branched hemicellulose
1509 (m)	Aromatic C—O stretching mode for lignin; guayacyl ring of lignin; lignocellulose
1445 (m)	O—CH_3
1373 (m)	C—H stretch of cellulose
1315–1316 (m)	CH_2 wagging
1229 (m)	C—O—C stretching
1159 (m)	Antisymmetric stretching C—O—C glycoside; C—O—C β-1, 4 glycosil linkage of cellulose
1105 (m)	C—O vibration of crystalline cellulose; glucose ring stretch from cellulose
1029–1035 (m)	C—O vibration of cellulose
889–896 (m)	Amorphous cellulose vibration; glucose ring stretch
700–900 (m)	C—H
967,1271,855 (m)	—CH_3

for providing better reinforcement for composite materials using these nanofibers (Alemdar & Sain, 2008b; Bhatnagar & Sain, 2005; Rong, Zhang, Liu, Yang, & Zeng, 2001).

FT-IR spectroscopy is a nondestructive method for examining the physico-chemical properties of lignocellulosic materials. The FT-IR spectra of (a) the raw materials, (b) purified pine needle fibers, (c) pine needle nanofibers (d) the trimethylchlorosilane treated NFC aerogel are shown in Fig. 5. Furthermore, the characteristic absorption peaks from the above samples were summarized in Table 2 (Esteves, Velez Marques, Domingos, & Pereira, 2013; Kahar, 2013; Liu, Sha, Cooper, & Fan, 2009; Pandey, 1999; Yang, Yan, Chen, Lee, & Zheng, 2007). The dominant peaks in the region between around 3325–3340 cm^{-1} and 2889–2915 cm^{-1} were due to stretching vibrations of O—H and C—H (Oh et al., 2005). The peak at 1509 in the spectrum of (a) the raw materials, which was attributed to Aromatic C—O stretching mode for lignin and guaiacol ring of lignin, disappeared completely in (b) purified pine needle fibers and (c) pine needle nanofibers. This indicated that the lignin was well removed from the newly prepared pine needle nanofibers by the $NaClO_2$ treatment. The prominent peak at 1727 cm^{-1} in the (a) the raw materials was attributed to either the acetyl and uronic ester groups of the hemicelluloses or the ester linkage of carboxylic group of the ferulic and p-coumeric acids of the lignin and/or hemicelluloses. This peak disappeared completely in the chemically treated pine needles because of the removal of the most hemicelluloses and lignin from the pine needles by applying the chemical extraction (Sain & Panthapulakkal, 2006). Interestingly, no difference between the spectrum of cellulose nanofibers obtained under different ultrasonic output powers and chemical-purified cellulose fibers was found. This result suggested that the molecular structures of cellulose remained unchanged in the case of ultrasonic treatment. The increase of the band at 889–896 cm^{-1} in the chemically treated pine needles illustrates the typical structure of cellulose. Furthermore, after the surface modification, (d) the trimethylchlorosilane treated NFC aerogel showed visible absorption peaks at 2967, 1271 and 855 cm^{-1}, which correspond to —CH_3 terminal groups. The adsorption peaks of the O—H bond weakened as the trimethylchlorosilane modified NFC aerogel became hydrophobic with fewer adsorbed water molecules. With this treatment, the —OH groups were replaced with —$OSi(CH_3)_3$ groups from trimethylchlorosilane to make the aerogels hydrophobic (Wei, Lu, & Chang, 2008).

Investigating the thermal properties of reinforcing materials is important in order to identify their applicability for biocomposite processing at high temperatures (Alemdar & Sain, 2008a). The

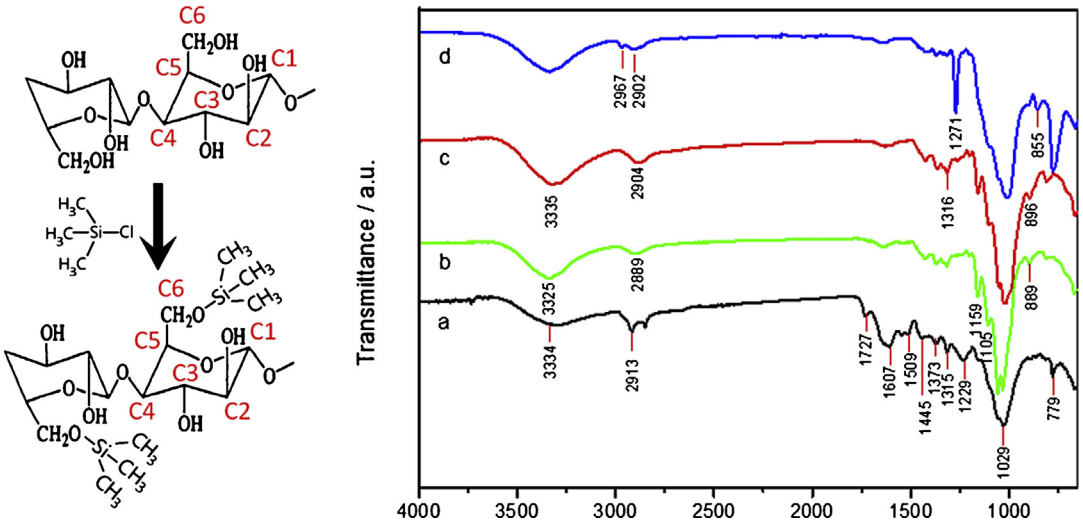

Fig. 5. FT-IR spectra of (a) the raw materials, (b) chemical-purified cellulose fibers, (c) pine needle nanofibers, (d) the trimethylchlorosilane treated NFC aerogel.

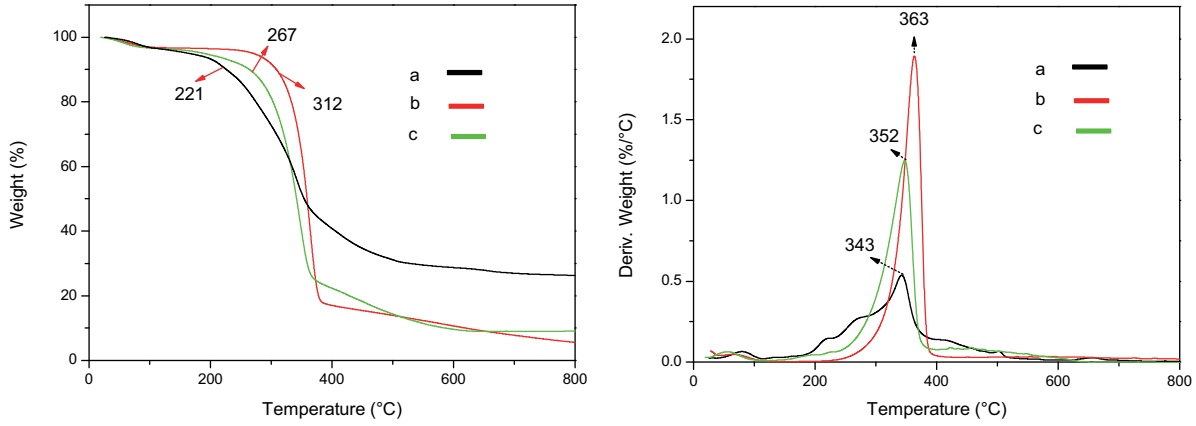

Fig. 6. TGA and DTG thermograms of (a) the raw material, (b) chemical-purified cellulose fibers and (c) pine needle nanofibers, under nitrogen atmosphere.

thermogravimetry (TGA) and derivative thermogravimetry (DTG) results obtained from (a) the raw material, (b) chemical-purified cellulose and (c) pine needle nanofibers are shown in Fig. 6. It was clearly that a small weight loss was found in the range of 25–120 °C due to the evaporation of the humidity of the materials or low molecular weight compounds remaining from the isolation procedures in all TGA and DTG curves (Kumar, Negi, Choudhary, & Bhardwaj, 2014; Soares, Camino, & Levchik, 1995; Xiao, Sun, & Sun, 2001). The onset of weight loss of the main step of degradation lain at 221, 267, and 312 °C for (a) the raw material, (b) chemical-purified cellulose and (c) pine needle nanofibers, respectively in TGA. In terms of thermal degradation, the three samples in the order of the easiest to the most difficult to degrade were a > c > b. The rate of degradation reached its peak at 343, 363 and 352 °C for (a) the raw material, (b) chemical-purified cellulose and (c) pine needle nanofibers, respectively in DTG. The thermal stability of (b) chemical-purified cellulose and (c) pine needle nanofibers is higher than that of (a) the raw material from the result of data analyses. It can be concluded that the higher temperature of thermal decomposition and lesser obtained residual mass of the fibers was contributed to the removal of hemicelluloses (Hemicellulose appears a random, amorphous structure, rich of branches, which are very easy to be removed from the main stem and to degrade to volatiles evolving out at low temperatures.) and lignin (Lignin is full of aromatic rings with various branches.) from the fibers and higher crystallinity of the cellulose after chemi-mechanical treatment (Nguyen, Zavarin, & Barrall, 1981; Yang et al., 2007). Furthermore, thermal degradation of pine needle nanofibers occurred at a lower temperature within broader ranges of temperature and exhibited lower thermal stability than chemical-purified cellulose due to their nano-sizes, greater number of free ends in the chain of pine needle nanofibers, and may show drastic reduction in the molecular weight (Kumar et al., 2014). Therefore, the nanofibers exhibited enhanced thermal properties, making them promising candidates for the application in thermoplastic composites.sds

3.2.1. *Fabrication of nanofiber ultralight flexible aerogels and hydrophobic nanofiber aerogels*

The condensed cellulose nanofibrillated hydrogels were collected. After freeze-drying the hydrogels, highly flexible nanofiber aerogels were fabricated. Fig. 7a shows nanofiber highly flexible aerogels, which can be repeatedly bent without destroying their structural integrity. Fig. 7b exhibits ultralight nanofiber aerogels, which had a white appearance and a bulk density of 3.12 mg/cm^{-3}. Thus, the separated nanofibrils can be easily stored and transported. These findings also verified that the highly flexible and low-density nanofiber flexible aerogels containing pine needle nanofibers were successfully prepared. Such nanofiber aerogels are expected to be used in various fundamental and applied research fields, such as nanofiber templates for hollow inorganic tubes, water purification, catalysis, sensing, separation, filtration, tissue engineering, and packaging materials (Deng, Zhou, Du, van Kasteren, & Wang, 2009).

The wettability of the uncoated and the hydrophobic aerogel were evaluated by static WCA measurements (Fig. 8). WCA of the pristine aerogel was 5° according to (a). The WCA of the samples treated with trimethylchlorosilane increased to 135° according to (b), which is an unmistakable sign for hydrophobicity. The modification by trimethylchlorosilane contributed to the formation of a low-energy surface of the cellulose aerogel due to the replacement of surface hydroxyl groups on the cellulose with plentiful —Si—$(CH_3)_3$ groups. Moreover, it showed that (c) photographs of

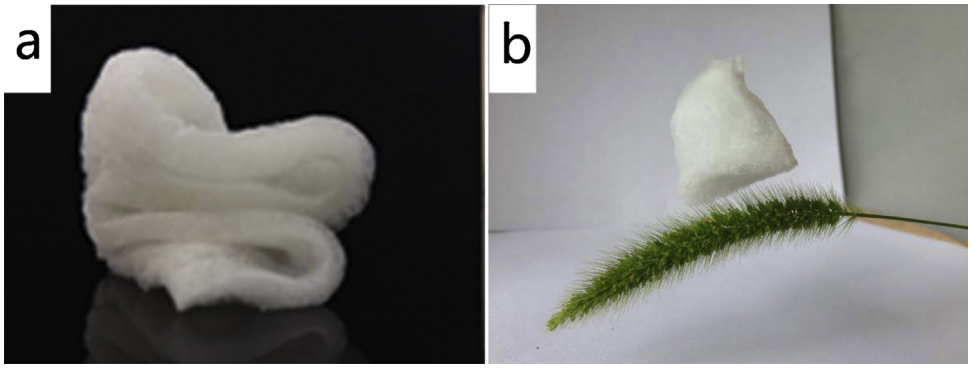

Fig. 7. (a) The nanofiber highly flexible aerogels were bent and folded without destroying their structural integrity, (b) the nanofiber ultralight aerogels were placed on dog tail grass.

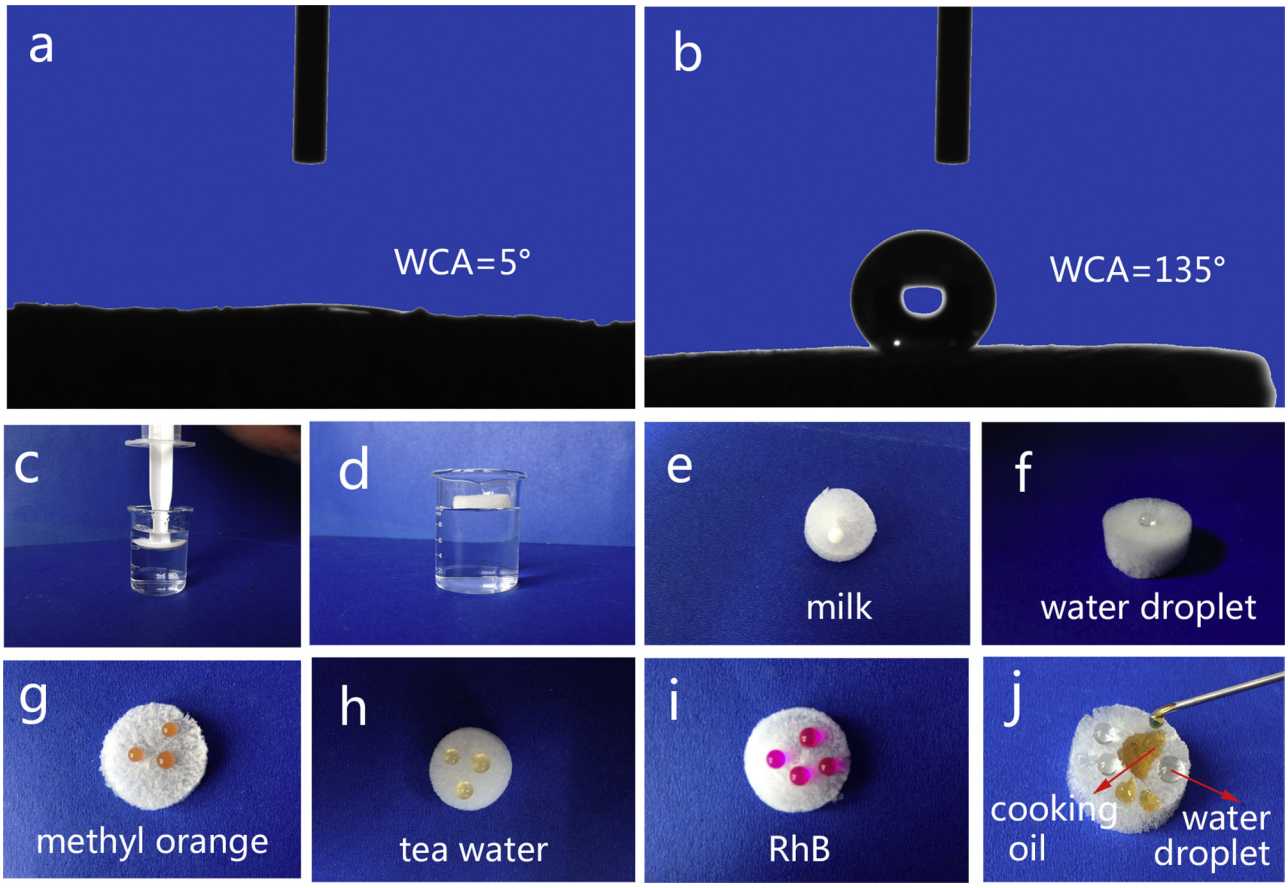

Fig. 8. Water contact angle (a) on the surface of the uncoated aerogel and (b) on the surface of the coated aerogel; (c) photographs of the coated aerogel was been pressed into water and (d) floated on the water surface; photographs of the static (e) milk, (f) water droplet, (g) methyl orange, (h) tea water, (i) RhB, and (j) cooking oil on the coated aerogel.

the coated aerogel was pressed into water and (d) floated on the water surface. The treated aerogel had hydrophobic for many other types of polar solvent such as the static (e) milk, (h) tea water, (f) drop, (i) RhB and (g) methyl orange in Fig. 8. Especially, it can rest on water droplet and at the same time absorb oil ((h) cooking oil and drop). The trimethylchlorosilane treated NFC aerogel might be an ideal candidate for highly efficient water-oil separation substances for oil spills (Cervin et al., 2012; Xue, Cao, Liu, Feng, & Jiang, 2014).

Fig. S2 shows the nitrogen adsorption–desorption isotherms, BJH pore size distribution, the specific surface areas, total pore volume and average pore diameter of NFC aerogels. In Fig. S2, NFC aerogels exhibit type IV adsorption isotherms according to the IUPAC classification, which indicate the presence of mesopores (Gregg, Sing, & Salzberg, 1967; Rouquerol et al., 1994). The desorption cycles of the isotherms exhibited a hysteresis loop which is generally attributed to the capillary condensation occurring in the mesopores. The pore diameter distributions was evaluated from the desorption branch of nitrogen isotherms by using the Barrett–Joyner–Halenda (BJH) method. The pore sizes of NFC aerogels was within the range 1–60 nm, and mainly consisted of micropores (<2 nm) and mesopores (2–50 nm). The specific surface areas, average pore diameter and total pore volume of NFC aerogel were 20.0927 m^2/g, 25.4465 nm, and 0.07762 m^3/g, respectively.

Mechanical property of NFC aerogels are summarized in Table S1. The NFC aerogels exhibit ductile behavior, can be compressed to large strains (>70%, see Fig. S3) and have low compression strength (37 kPa). As shown in Fig. S4, the modified NFC aerogel could stably float on the surface of the water. Subsequently, the modified aerogel could persistently stay on the oil layer under gravity after being put in the oil/water mixture. The oil absorbed cellulose aerogel is removed easily by simply squeezing it. The aerogels combine both hydrophobic and oleophilic properties and prove to be very efficient in removing oil from a water surface with an excellent selectivity and recyclability. Moreover, this aerogel could absorbed 52 times oil than that of its own weight without any collapse in oil (see in detail Movie S1).

4. Conclusions

In the present work, cellulose nanofibers were extracted from pine needles by chemical-mechanical treatments. Experimental results showed that the diameters of the produced pine needle nanofibers were within the range of 30–70 nm. Chemical analysis and FTIR measurements of the fibers revealed that the partial hemicelluloses and lignin were due to the success of the chemical treatment applied. The crystallinity of the cellulose was increased by 7.61% for the pine needle nanofibers. The nanofibers exhibited enhanced thermal properties, thus making them promising candidates for the use in thermoplastic composites. Furthermore, highly flexible and ultralight pine needle nanofibers and hydrophobic coating of pine needle nanofibers aerogels were manufactured.

Acknowledgments

This work was financially supported by The National Natural Science Foundation of China (grant no. 31270590), China Postdoctoral Science Foundation funded project (2013M540263), and Doctoral Candidate Innovation Research Support Program of Science & Technology Review (kjdb2012006).

Appendix A. Supplementary data

Supplementary data associated with this article can be found, in the online version, at http://dx.doi.org/10.1016/j.carbpol.2014.11.041.

References

Abe, K., Iwamoto, S., & Yano, H. (2007). Obtaining cellulose nanofibers with a uniform width of 15 nm from wood. *Biomacromolecules*, *8*(10), 3276–3278.

Abe, K., & Yano, H. (2009). Comparison of the characteristics of cellulose microfibril aggregates of wood, rice straw and potato tuber. *Cellulose*, *16*(6), 1017–1023.

Alemdar, A., & Sain, M. (2008a). Biocomposites from wheat straw nanofibers: Morphology, thermal and mechanical properties. *Composites Science and Technology*, *68*(2), 557–565.

Alemdar, A., & Sain, M. (2008b). Isolation and characterization of nanofibers from agricultural residues – Wheat straw and soy hulls. *Bioresource Technology*, *99*(6), 1664–1671.

Bang, J. H., & Suslick, K. S. (2010). Applications of ultrasound to the synthesis of nanostructured materials. *Advanced Materials*, *22*(10), 1039–1059.

Bhatnagar, A., & Sain, M. (2005). Processing of cellulose nanofiber-reinforced composites. *Journal of Reinforced Plastics and Composites*, *24*(12), 1259–1268.

Bodin, A., Ahrenstedt, L., Fink, H., Brumer, H., Risberg, B., & Gatenholm, P. (2007). Modification of nanocellulose with a xyloglucan–RGD conjugate enhances adhesion and proliferation of endothelial cells: Implications for tissue engineering. *Biomacromolecules*, *8*(12), 3697–3704.

Cervin, N. T., Andersson, L. A., Ng, J. B. S., Olin, P., Bergström, L., & Wa¨gberg, L. (2013). Lightweight and strong cellulose materials made from aqueous foams stabilized by nanofibrillated cellulose. *Biomacromolecules*, *14*(2), 503–511.

Cervin, N. T., Aulin, C., Larsson, P. T., & Wågberg, L. (2012). Ultra porous nanocellulose aerogels as separation medium for mixtures of oil/water liquids. *Cellulose*, *19*(2), 401–410.

Chen, P., Yu, H., Liu, Y., Chen, W., Wang, X., & Ouyang, M. (2013). Concentration effects on the isolation and dynamic rheological behavior of cellulose nanofibers *via* ultrasonic processing. *Cellulose*, *20*(1), 149–157.

Chen, Y., Liu, C., Chang, P. R., Cao, X., & Anderson, D. P. (2009). Bionanocomposites based on pea starch and cellulose nanowhiskers hydrolyzed from pea hull fibre: Effect of hydrolysis time. *Carbohydrate Polymers*, *76*(4), 607–615.

Cheng, Q., Wang, S., & Han, Q. (2010). Novel process for isolating fibrils from cellulose fibers by high-intensity ultrasonication. II. Fibril characterization. *Journal of Applied Polymer Science*, *115*(5), 2756–2762.

Deng, M., Zhou, Q., Du, A., van Kasteren, J., & Wang, Y. (2009). Preparation of nanoporous cellulose foams from cellulose-ionic liquid solutions. *Materials Letters*, *63*(21), 1851–1854.

Esteves, B., Velez Marques, A., Domingos, I., & Pereira, H. (2013). Chemical changes of heat treated pine and eucalypt wood monitored by FTIR. *Maderas. Ciencia y Tecnología (AHEAD)*, *15*(2), 245–258.

Gregg, S. J., Sing, K. S. W., & Salzberg, H. (1967). Adsorption surface area and porosity. *Journal of the Electrochemical Society*, *114*(11), 279C.

Habibi, Y., Lucia, L. A., & Rojas, O. J. (2010). Cellulose nanocrystals: Chemistry, self-assembly, and applications. *Chemical Reviews*, *110*(6), 3479–3500.

Hornsby, P., Hinrichsen, E., & Tarverdi, K. (1997). Preparation and properties of polypropylene composites reinforced with wheat and flax straw fibres: Part I fibre characterization. *Journal of Materials Science*, *32*(2), 443–449.

Huang, Z.-M., Zhang, Y.-Z., Kotaki, M., & Ramakrishna, S. (2003). A review on polymer nanofibers by electrospinning and their applications in nanocomposites. *Composites Science and Technology*, *63*(15), 2223–2253.

Ifuku, S., & Saimoto, H. (2012). Chitin nanofibers: Preparations, modifications, and applications. *Nanoscale*, *4*(11), 3308–3318.

Kahar, P. (2013). Synergistic effects of pretreatment process on enzymatic digestion of rice straw for efficient ethanol fermentation. In M. Petre (Ed.), *Environmental biotechnology – New approaches and prospective applications*. Janeza Trdine 9, 51000 Rijeka, Croatia: InTech.

Khan, R. A., Salmieri, S., Dussault, D., Uribe-Calderon, J., Kamal, M. R., Safrany, A., et al. (2010). Production and properties of nanocellulose-reinforced methylcellulose-based biodegradable films. *Journal of Agricultural and Food Chemistry*, *58*(13), 7878–7885.

Kim, C.-W., Kim, D.-S., Kang, S.-Y., Marquez, M., & Joo, Y. L. (2006). Structural studies of electrospun cellulose nanofibers. *Polymer*, *47*(14), 5097–5107.

Klemm, D., Kramer, F., Moritz, S., Lindström, T., Ankerfors, M., Gray, D., et al. (2011). Nanocelluloses: A new family of nature-based materials. *Angewandte Chemie International Edition*, *50*(24), 5438–5466.

Klemm, D., Schumann, D., Kramer, F., Heßler, N., Hornung, M., Schmauder, H.-P., et al. (2006). Nanocelluloses as innovative polymers in research and application. In *Polysaccharides II*. Berlin: Springer.

Kumar, A., Negi, Y. S., Choudhary, V., & Bhardwaj, N. K. (2014). Characterization of cellulose nanocrystals produced by acid-hydrolysis from sugarcane bagasse as agro-waste. *Journal of Materials Physics and Chemistry*, *2*(1), 1–8.

Li, D., & Xia, Y. (2004). Electrospinning of nanofibers: Reinventing the wheel? *Advanced Materials*, *16*(14), 1151–1170.

Li, R., Fei, J., Cai, Y., Li, Y., Feng, J., & Yao, J. (2009). Cellulose whiskers extracted from mulberry: A novel biomass production. *Carbohydrate Polymers*, *76*(1), 94–99.

Liu, H., Sha, W., Cooper, A. T., & Fan, M. (2009). Preparation and characterization of a novel silica aerogel as adsorbent for toxic organic compounds. *Colloids and Surfaces A: Physicochemical and Engineering Aspects*, *347*(1), 38–44.

Lu, Y., Sun, Q., She, X., Xia, Y., Liu, Y., Li, J., et al. (2013). Fabrication and characterisation of α-chitin nanofibers and highly transparent chitin films by pulsed ultrasonication. *Carbohydrate Polymers*, *98*(2), 1497–1504.

Nguyen, T., Zavarin, E., & Barrall, E. M. (1981). Thermal analysis of lignocellulosic materials: Part I. Unmodified Materials. *Journal of Macromolecular Science – Reviews in Macromolecular Chemistry*, *20*(1), 1–65.

Nishiyama, Y., Sugiyama, J., Chanzy, H., & Langan, P. (2003). Crystal structure and hydrogen bonding system in cellulose Iα from synchrotron X-ray and neutron fiber diffraction. *Journal of the American Chemical Society*, *125*(47), 14300–14306.

Oh, S. Y., Yoo, D. I., Shin, Y., Kim, H. C., Kim, H. Y., Chung, Y. S., et al. (2005). Crystalline structure analysis of cellulose treated with sodium hydroxide and carbon dioxide by means of X-ray diffraction and FTIR spectroscopy. *Carbohydrate Research*, *340*(15), 2376–2391.

Pandey, K. (1999). A study of chemical structure of soft and hardwood and wood polymers by FTIR spectroscopy. *Journal of Applied Polymer Science*, *71*(12), 1969–1975.

Rong, M. Z., Zhang, M. Q., Liu, Y., Yang, G. C., & Zeng, H. M. (2001). The effect of fiber treatment on the mechanical properties of unidirectional sisal-reinforced epoxy composites. *Composites Science and Technology*, *61*(10), 1437–1447.

Rouquerol, J., Avnir, D., Fairbridge, C., Everett, D., Haynes, J., Pernicone, N., et al. (1994). Recommendations for the characterization of porous solids (Technical Report). *Pure and Applied Chemistry*, *66*(8), 1739–1758.

Sain, M., & Panthapulakkal, S. (2006). Bioprocess preparation of wheat straw fibers and their characterization. *Industrial Crops and Products*, *23*(1), 1–8.

Saito, T., Kimura, S., Nishiyama, Y., & Isogai, A. (2007). Cellulose nanofibers prepared by TEMPO-mediated oxidation of native cellulose. *Biomacromolecules*, *8*(8), 2485–2491.

Shinoda, R., Saito, T., Okita, Y., & Isogai, A. (2012). Relationship between length and degree of polymerization of TEMPO-oxidized cellulose nanofibrils. *Biomacromolecules*, *13*(3), 842–849.

Soares, S., Camino, G., & Levchik, S. (1995). Comparative study of the thermal decomposition of pure cellulose and pulp paper. *Polymer Degradation and Stability*, *49*(2), 275–283.

Sun, Y., Mayers, B., Herricks, T., & Xia, Y. (2003). Polyol synthesis of uniform silver nanowires: A plausible growth mechanism and the supporting evidence. *Nano Letters*, *3*(7), 955–960.

Suslick, K. S. (1998). *Sonochemistry. Kirk-Othmer Encyclopedia of Chemical Technology*. John Wiley & Sons.

Thakur, V., & Singha, A. (2011). Physicochemical and mechanical behavior of cellulosic pine needle-based biocomposites. *International Journal of Polymer Analysis and Characterization*, *16*(6), 390–398.

Tischer, P. C. F., Sierakowski, M. R., Westfahl, H., Jr., & Tischer, C. A. (2010). Nanostructural reorganization of bacterial cellulose by ultrasonic treatment. *Biomacromolecules*, *11*(5), 1217–1224.

Valo, H., Arola, S., Laaksonen, P., Torkkeli, M., Peltonen, L., Linder, M. B., et al. (2013). Drug release from nanoparticles embedded in four different nanofibrillar cellulose aerogels. *European Journal of Pharmaceutical Sciences*, *50*(1), 69–77.

Wei, T.-Y., Lu, S.-Y., & Chang, Y.-C. (2008). Transparent, hydrophobic composite aerogels with high mechanical strength and low high-temperature thermal conductivities. *Journal of Physical Chemistry B*, *112*(38), 11881–11886.

Xiao, B., Sun, X., & Sun, R. (2001). Chemical, structural, and thermal characterizations of alkali-soluble lignins and hemicelluloses, and cellulose from maize stems, rye straw, and rice straw. *Polymer Degradation and Stability*, *74*(2), 307–319.

Xue, Z., Cao, Y., Liu, N., Feng, L., & Jiang, L. (2014). Special wettable materials for oil/water separation. *Journal of Materials Chemistry A*, *2*(8), 2445–2460.

Yang, H., Yan, R., Chen, H., Lee, D. H., & Zheng, C. (2007). Characteristics of hemicellulose, cellulose and lignin pyrolysis. *Fuel*, *86*(12), 1781–1788.

Zeiger, B. W., & Suslick, K. S. (2011). Sonofragmentation of molecular crystals. *Journal of the American Chemical Society*, *133*(37), 14530–14533.

Zhang, C.-L., & Yu, S.-H. (2014). Nanoparticles meet electrospinning: Recent advances and future prospects. *Chemical Society Reviews*, *43*(13), 4423–4448.

Zhang, Z., Sèbe, G., Rentsch, D., Zimmermann, T., & Tingaut, P. (2014). Ultralightweight and flexible silylated nanocellulose sponges for the selective removal of oil from Water. *Chemistry of Materials*, *26*(8), 2659–2668.

Zhao, H.-P., Feng, X.-Q., & Gao, H. (2007). Ultrasonic technique for extracting nanofibers from nature materials. *Applied Physics Letters*, *90*(7), 073112.